Optimization and continuous-flow operation of electrochemically mediated selective formate separation by polyvinyl ferrocene/graphene oxide electrodes

Polat, Sevgi; Kortlever, Ruud; Eral, Hüseyin Burak

DOI
10.1016/j.cej.2023.146169

Publication date
2023

Document Version
Final published version

Published in
Chemical Engineering Journal

Chemical Engineering Journal 475 (2023) 146169

Contents lists available at ScienceDirect

Chemical Engineering Journal

journal homepage: www.elsevier.com/locate/cej

Optimization and continuous-flow operation of electrochemically mediated selective formate separation by polyvinyl ferrocene/graphene oxide electrodes

Sevgi Polat [a,b,*], Ruud Kortlever [c], Hüseyin Burak Eral [a]

[a] Complex Fluid Processing Section, Process & Energy Department, Faculty of Mechanical, Maritime and Materials Engineering, Delft University of Technology, 2628 CB Delft, The Netherlands
[b] Chemical Engineering Department, Faculty of Engineering, Marmara University, 34854 İstanbul, Turkey
[c] Large-Scale Energy Storage Section, Process & Energy Department, Faculty of Mechanical, Maritime and Materials Engineering, Delft University of Technology, 2628 CB Delft, The Netherlands

ARTICLE INFO

Keywords:
Electrochemical separation
Cell design
Optimization
Resource recovery
Formate

ABSTRACT

Electrochemical carbon dioxide (CO_2) reduction is a promising route to convert intermittent renewable energy into fuels and valuable chemical products. Separation of CO_2 reduction products by ion-selective electrochemical technology may play a decisive role in the pursuit of commercially viable CO_2 reduction processes. Selective separation of formate, one of the main CO_2 reduction products, is assessed in the present study in an electrochemical flow cell with symmetric redox-active polyvinyl ferrocene (PVF) functionalized graphene oxide (GO) electrodes. First, experimental parameters such as the PVF/GO ratio, sonication time, and ultrasonic amplitude, were optimized in the electrode preparation process to improve the formate adsorption efficiency on a lab scale (1 × 2 cm electrodes) under static conditions. The electrochemical and morphological characteristics of the electrodes were investigated by cyclic voltammetry and scanning electron microscopy. To demonstrate continuous-flow operation, an electrosorption flow cell (8 × 8 cm) providing inline measurements was constructed. The flow cell results showed selectivity at > 5.5 toward the removal of formate from an electrolyte containing perchlorate at an excess of 30 times the normal value. The performance of the electrosorption cell was also tested using a mixture of methanol, ethanol, formate, and acetaldehyde produced in a CO_2 reduction electrolyzer. In this demonstration, formate separation was achieved with a selectivity of > 4.0. The results suggest that the optimized design of the electrochemical cell and operation conditions of the flow platform pave the way for scaling up selective formate separation with PVF/GO electrodes.

1. Introduction

Climate change has been one of the major societal challenges in recent history and will continue to be for the coming decades. The global surface temperature has increased by 0.2 °C per decade for the past 30 years, and this trend is predicted to continue at an increasing rate in years to follow [1–3]. A limit of a 2 °C global temperature increase was proposed to prevent dramatic and irreversible effects of climate change, such as an overwhelming rise in sea level, record-breaking droughts, and an overwhelming loss of biodiversity. Recent studies have estimated that the actual rise is going to overshoot the aforementioned 2 °C limit enormously if no action is taken [4–6]. Carbon dioxide (CO_2) is a major contributor to climate change. Over the past decade, global CO_2 emissions in the atmosphere have increased more than ever with values of 421 ppm in 2022, and this trend is expected to continue [7–9]. Roughly, 90% of human-made CO_2 emissions are the result of burning fossil fuels for industry [6], making fossil fuels by far the largest contributor to CO_2 related climate change [10]. As the effects of climate change become more visible, the necessity to reduce the use of fossil fuels increases. However, humans worldwide depend on fossil fuels for energy, fuel, transport, and carbon-based commodity chemical production, which makes fossil fuel reduction an enormous challenge. Nevertheless, worldwide support to fight climate change has increased significantly, which has made agreements more acceptable on reducing CO_2 emissions

* Corresponding author at: Complex Fluid Processing Section, Process & Energy Department, Faculty of Mechanical, Maritime and Materials Engineering, Delft University of Technology, 2628 CB Delft, The Netherlands.
E-mail address: S.Polat@tudelft.nl (S. Polat).

https://doi.org/10.1016/j.cej.2023.146169
Received 14 June 2023; Received in revised form 11 September 2023; Accepted 18 September 2023
Available online 19 September 2023

by using alternatives to fossil fuels. A circular economy without any CO_2 being released into the atmosphere would be ideal [8,11]. Although the switch to renewable energy sources appears to be promising, there are still some major challenges to address [12]. New methods for producing carbon-based products must be identified, the production of renewable energy must become more effective, energy storage possibilities must be improved, and the back conversion and utilization of CO_2 must be improved. All of these aforementioned points will play an important role in creating a circular economy in a CO_2 neutral future [13]. These changes could be accomplished by reducing energy consumption by increasing efficiency through electrochemical CO_2 reduction, offering a viable route to produce circular fuel and carbon-based commodity chemicals [14–16]. By capturing the CO_2 that is produced by fuel combustion and industrial processes and using this to make new products and fuels, no new CO_2 would be released into the atmosphere, stopping any increase in CO_2 concentration, and helping to resolve the supply and demand issues. When fuels or chemical intermediates are produced using renewable energy sources, the potential energy is stored in the chemical bonds. These chemicals can then be stored when the demand is lower than the supply and can be converted back into energy when the supply is lower than the demand [17,18].

Even with these benefits, there are several issues that must be resolved in the process of electrocatalytic CO_2 reduction [19,20]. In principle, CO_2 reduction processes demand a significantly high overpotential. In addition to a high overpotential, the process suffers from low faradaic efficiency and poor selectivity of ions [21,22]. The poor solubility of CO_2 in the catholyte severely restricts the reaction rate, making CO_2 reduction unsuitable for large-scale use. Some efforts have been reported to overcome the low CO_2 solubility of aqueous electrolytes and eliminate mass-transfer limitation including the use of a humidified CO_2 input stream at the cathode compartment of the electrochemical reactor [19,23]. Nevertheless, operation with humidified CO_2 gaseous feed for continuous electroreduction to formate has resulted in general higher reactor voltages, which prevents efficient operation at high current densities [23]. Furthermore, liquid electrolytes dilute reduction products, which elevates the separation costs for product recovery. Moreover, if the obtained product from electrocatalytic CO_2 reduction is formate these ions will be mixed with other impurity ions from solutes [24–26]. Hence, improving product selectivity and efficiency is important for making electrochemical CO_2 reduction economically feasible; however, product separation is the most capital and energy intensive step and is often overlooked. In the separation of products from the electrochemical conversion of CO_2, product concentrations are in lower quantities compared to a large excess of ions (i.e. electrolytes [26–28]; therefore, selectively separating products from a homogeneous mixture is challenging [26,29].

Formate is a key product formed in CO_2 reduction; therefore, its separation from homogeneous reaction mixtures containing salts is extremely important in the pursuit for economically viable electrochemical CO_2 reduction. In addition, formate can be produced with a high selectivity at relatively low overpotentials [30]. Since the CO_2 reduction reaction is early in the development phase and it is necessary to continue research efforts to produce formate with high purity and high concentration an ion-selective separation method with high throughput and separation factors would be extremely beneficial. Commercially available separation methods, such as distillation, extraction, precipitation, and pervaporation have drawbacks, including, high energy requirements, poor removal of ions at low concentrations, and high operating costs [31,32]. Extensive research has been conducted to develop more affordable and effective processes, and some advanced separation technologies have been developed, investigated, and applied to address these issues. Among recently proposed technologies, pseudocapacitive deionization (PCDI) is an electrochemical separation technique that uses redox-active compounds to selectively capture ions. These organometallic compounds are deposited on the surface of a carbon electrode and PCDI would offer a feasible solution to the issues faced because of the fast kinetics of the processes, control by electrical potential, lower footprint, modularity, scalability, and reversibility [33–36].

In addition, PCDI does not require additional chemicals or additional solvents for the regeneration step, which makes it extremely useful in terms of water economy and downstream waste sustainability. Su et al. [29] have reported a pseudocapacitive electrode based on metallocene ferrocene being able to selectively separate carboxylates, sulfonates, and phosphonates from an aqueous solution. They were able to selectively separate formate from a solution containing a ratio of 1:30 formate to competing anions and to demonstrate that this technique has great potential. These advantages have brought to the forefront a process by which to selectively separate formate ions from competing ions [35]; however, the process remains limited to within a small scale under static conditions. Ideally, these batch process should be converted continuous to increase throughput.

In the present study, the PVF/GO electrode preparation process was first optimized to achieve the highest number of active surface sites and the greatest adsorption efficiency to facilitate scale up the selective separation process. The electrodes were characterized electrochemically and morphologically. Moreover, a continuous-flow separation setup using the electrodes with optimized adsorption efficiency yet larger (5 × 5 cm) projected surface area was developed for ion-specific selection. Ion-specific separation of formate ions using this electrosorption system with PVF/GO electrodes was demonstrated. In the presence of excess perchlorate electrolyte, selectivity of formate separation was quantified. In addition, the operation of the designed system was demonstrated with a characteristic solution from CO_2 reduction process. The results of the present study address resource separation from electrochemically reducing CO_2.

2. Experimental section

2.1. Materials

Polyvinyl ferrocene (PVF, CAS number 34801–99-5) and graphene oxide (GO) were obtained from Polysciences and Graphenea, respectively. Dimethylformamide (DMF, CAS number 68–12-2), potassium formate (CAS number 590–29-4), and lithium perchlorate (CAS number 7791–03-9) were purchased from Sigma Aldrich. All chemicals were used as received without any further purification. Toray carbon paper (CP, TGP-H-60) was supplied from Alfa Aesar. Ultrapure water (Millipore MilliQ IQ 7000) was used to prepare the solutions.

2.2. Experimental methods

Fig. S1 provides a flow diagram that shows the experimental stages of the process. The experiments were conducted using two different scales under static (1 × 2 cm) and continuous-flow (8 × 8 cm) conditions.

2.2.1. Electrode manufacturing

A series of electrodes was prepared in which the compositions of PVF and GO were varied. At first, based on the wt% desired for the electrode, specific mass of PVF and GO were loaded into a 20-mL glass vial. An appropriate amount of DMF (10 mL) used as the solvent was then added to the vial. A Cole-Parmer ultrasonic homogenizer with a 0.5-in-diameter immersion ultrasonic probe was used on the solution to provide homogenous and high-quality dispersion. The tip of the ultrasonic probe was lowered into the vial and the vial was closed with the parafilm to avoid any interactions from the surroundings. The sonication was done in an ice bath to prevent the evaporation of the solvent and avoid extra heat generation. Application of the ultrasound for homogenization, mixing, dispersion, and coating is well-known and has been explored in lots of papers in recent years [37–40]. Our previous study has also highlighted the ultrasound-intensified fabrication process for the

polyvinyl ferrocene/carbon nanotube electrodes [41,42]. The different amplitude percentages, ranging from 20 to 60%, and sonication times, ranging from 30 to 90 min, were applied to determine an optimal sonication program with the highest dispersion level. All of the prepared mixtures using different PVF/GO ratios were then sonicated at a constant frequency but at different amplitudes and durations. After preparing the solutions, the working electrodes were manufactured using Toray carbon paper. Several 1- x 2-cm carbon paper electrodes were prepared to be used as the surface of the working electrode, where the surface area used for drop casting was 1 × 1 cm for lab-scale experiments. The solution (50 μL) was drop casted onto the one side of the electrode surface. The wet electrodes were then dried in the oven for 60 min at 30 °C. Electrochemical measurements were then taken and morphological characterization conducted on the dried electrodes. The electrodes were 8 × 8 cm with an exposed surface of 5 × 5 cm. They were functionalized in 250 μL PVF/GO solution.

2.2.2. Electrochemical measurements and characterization

A three-electrode setup was used for the cyclic voltammetry (CV) measurements that comprised Ag/AgCl that acted as a reference electrode, a platinum-based electrode that acted as a counter electrode, and the PVF/GO electrode that acted as a working electrode. A Biologic SP-200 potentiostat was used to perform the CV measurements and Biologic EC-lab peak-analysis tool was used to analyze the results obtained from the potentiostat. The electrode characterization was performed in 0.1 M $LiClO_4$ solution prepared with argon purging to remove the extra oxygen in the solution at a scan rate of 5 mV/s at room temperature. (1) shows the relation between the charge and the measured current:

$$Q = \int_{t_1}^{t_2} Idt = \frac{1}{\nu}\int_{E_1}^{E_2} IdE \tag{1}$$

where Q is the charge (C), ν is the sweep rate (V/s) and E_1 and E_2 are the potentials where the anodic peak starts and ends (V). The number of active surface sites can be determined from the charge as shown in the following (2):

$$N_{sites} = \frac{Q}{nF} \tag{2}$$

where N_{sites} is the number of activated surface sites in moles, Q is the calculated charge (C), F is the Faraday constant (C/mol), and n *is* the number of electrons transferred per reaction. For every ferrocene unit that is oxidized, one electron is produced meaning that n = 1 for this reaction. The performance of the working electrodes with respect to formate adsorption and desorption was tested using chronoamperometry. A potential of 0.6 V and 0.2 V vs. Ag/AgCl was applied for 15 min for adsorption and desorption experiments, respectively. The amount of adsorbed formate was estimated by applying the following formula:

$$N_{ads} = (C_0 - C_1) \times V_e \tag{3}$$

The difference between the initial concentration (C_0), and the concentration after adsorption (C_1), multiplied by the electrolyte volume (V_e) resulted in the amount of adsorbed formate (N_{ads}) by the redox-active material on the electrode surface. High-performance liquid chromatography (HPLC, Agilent 1260 Infinity) was used to determine the concentration of formate ions before and after electrosorption. The liquid samples were filtered before HPLC analysis using a 0.22 μm membrane filter. Aminex HPX 87-H columns (Biorad) were used with a 0.600 mL/min flow rate of an aqueous 1 mM H_2SO_4 eluent. The column was maintained at 60 °C, and the injection volume was 10 μL.

In addition to the electrochemical characterization, the morphological characteristics of the PVF/GO electrodes were investigated by scanning electron microscopy (SEM, Jeol JSM 6500F) with an accelerating voltage of 15 kV to better characterize the PVF/GO electrodes.

2.2.3. Design of experiments

To fabricate the PVF/GO electrodes with the desired properties (i.e., the highest number of active surface sites and highest formate adsorption efficiency), the experimental design approach was used. The variables that would affect PVF/GO dispersion quality and interactions needed to be investigated. The PVF/GO ratio (A), sonication time (B), and ultrasonic amplitude (C) were chosen as the input variables. The number of active surface sites and adsorption efficiency were the responses. A Box–Behnken design combined with the response surface method was used to generate the study plan. Each parameter was varied over three levels that represented the upper (+1), medium (0), and lower (-1) limits of each. The data representing the upper and lower limits of each were then selected based on preliminary experimental results (ultrasonic amplitude 10–80% and sonication time 15–180 min). The electrodes used in design experiments were 1x2 cm, where the surface area exposed to the electrolyte was 1x1 cm. Each experiment in the study was conducted at least twice. The levels and ranges of variables used in this study are shown in Table 1.

Based on a three-factor, three-level Box–Behnken design, a total of 15 experiments with varying conditions have been designed using by Design Expert (https://www.statease.com/software/design-expert/) to investigate the correlation between the combined effects of the individual parameters and both responses. The designed experiments and their corresponding measured responses are presented in Table S1. After, the analysis of variance (ANOVA) technique was used to evaluate the significance of the parameters and the combined effect on both responses through their interaction. A second-order polynomial equation also known as second-order response surface model was used to investigate the predicted response and the process variable. The general form of this equation is as follows:

$$Y = \beta_0 + \sum_{i=1}^{k}\beta_i X_i + \sum_{i=1}^{k}\beta_{ii}X_i^2 + \sum_{i_{i=1}}^{k}\sum_{j>1}^{k}\beta_{ij}X_iX_j \tag{4}$$

where Y shows the predicted response, β_0 is the constant coefficient, β_i is the linear coefficient, β_{ii} is the quadratic coefficient, and β_{ij} is the interaction coefficient. The coefficients are calculated by analyzing the experimentally obtained data using multiple regression analysis into a second-order polynomial equation. Eventually, the genetic algorithm embedded with the design expert software was employed to calculate the optimum synthesis parameters and solve for the relevant predicted responses.

2.2.4. Architecture of electrochemical cell design and electrosorption setup

An electrosorption cell basically consists of two electrodes sandwiching a flow channel. As shown in Fig. 1a, when a potential is imposed across the electrodes, ions in water will be electrostatically attracted to the electrodes and the resulting effluent removed from the ions. Once the electrodes are saturated with ions, a short-circuit is applied to discharge the electrodes. Ions desorb from the electrode surface and the electrodes are regenerated. In the present study, the electrosorption cell designed using Rhinoceros 3D modelling software to provide continuous-flow and larger scale selective formate separation was a single-channel rectangular cell with water flowing between two rectangular acrylic plates. The cell was designed properly and was air and watertight, ensuring that all solution flowed through the cell and none was lost as a result of leakage. As depicted in Fig. 1b, the cell consisted of

Table 1
Range and levels of variables in Box–Behnken experimental design.

Design variable	Symbol	Range and levels		
		−1	0	1
PVF/GO Ratio	A	0.5	1	1.5
Sonication Time (min)	B	30	60	90
Ultrasonic Amplitude (%)	C	20	40	60

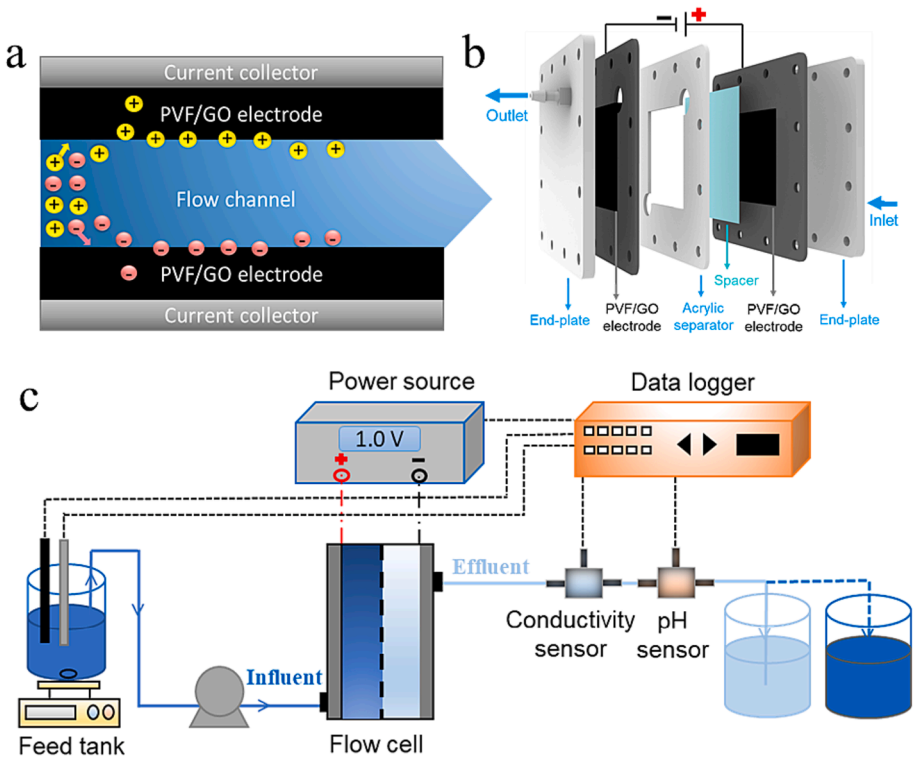

Fig. 1. (a) Schematic diagram showing preferred adsorption of formate ions across PVF/GO electrodes. (b) Exploded view of the electrochemical cell with PVF/GO electrodes, acrylic separator, and a spacer. (c) Schematic representation of electrosorption experimental setup.

two acrylic plates (80 × 80 × 4 mm) made using a laser cutter and placed parallel to each other. The internals of the electrosorption cell consisted of a separator, a pair of carbon paper electrodes, a polymer spacer, and titanium current collectors. The separator was made from acrylic and the rectangular cutout in the middle formed the channel. The separator thickness set the width of the channel (the thicker the separator, the wider the channel) and prevented short circuits between the electrodes; however, a larger width meant a lower electric field strength across the electrodes. To balance these two essential aspects, a separator width of 2 mm was considered in the study design. The spacer increased mass transfer through the channel by mixing the flowing feed solution and allowing for flow between the electrodes. A 0.205- and 0.05-mm-thick carbon paper and polymer spacer were used. Two titanium strips were stuck to inside of the endplates to function as current collectors. The holes within the separators, electrodes, and endplates allowed for in- and outflow. The inlet and outlet of the cell were positioned at the bottom and top of the cell, respectively. The cell was secured with bolts and nuts dispersed around the lid. The PVF/GO electrodes measured 5 × 5 cm. An electrosorption system for continuous-flow was then assembled, which comprised an electrochemical cell, peristaltic pump, influent and effluent containers (for adsorption and desorption process), a power supply, and probes for conductivity and pH. Fig. 1c provides a schematic of this system.

The feed solution from the feed tank entered the cell through tubes connected to the feed point bolts and directed into the space between the acrylic plates. The experiments began with a channel that was flushed with ultrapure water for at least 60 min. Next, the feed solution from the feed tank was drawn into the fully equipped electrosorption cell at a constant flow rate of 0.5 mL/min. Immediately after exiting the cell, conductivity and pH inline sensors were put in place to continuously measure effluent conductivity and pH and evaluate the formate ion adsorption/desorption performance of the PVF/GO electrodes under flow conditions. Power was supplied using a source meter (Keithley, SMU 2450) and ensured the mode of operation for the experiments (e.g., using constant voltage or constant current). The applied potential and the used electric current were measured, and the power outlet connected to a data logger to record the data. During the experiments the power supply was set to maintain a constant electrostatic potential difference of 1.0 V. While the solution was pumped through the cell, a potential was applied for a set time after which it was removed. The cell was charged by applying 1.0 V for 5 min followed by a discharging step at −1.0 V for 5 min. This cycle of applying and discharging voltage was repeated several times. The experiments were conducted five times, and each was repeated three times. High-performance liquid chromatography (HPLC) was used to measure samples from the effluent to determine the amount of formate adsorbed. The amount of formate removed per charge passed was determined. This represented the total charge efficiency for the process and calculated as:

$$\Lambda = \frac{q_{formate}}{q_{charge}} = \frac{Q\int(C_{in} - C)dt}{\int Idt/F} \quad (5)$$

where C_{in} and C are the initial and final anions/cations concentrations, Q is the volumetric flow rate, F is Faraday constant.

3. Results and discussion

3.1. Electrochemical and morphological characterization

The electrochemical characterization of the PVF/GO fabricated electrodes at different PVF/GO ratios, sonication times, and ultrasonic amplitude conditions was conducted using cyclic voltammetry (CV) to determine the functionality and relative performance of the electrodes. The CV measurements were conducted using a three-electrode setup in a 0.1 M $LiClO_4$ aqueous electrolyte solution; the representative CV curves are shown in Fig. 2.

When first observed, the general shapes of the CV curves for the PVF/GO electrodes were identical; however, after comparing the CVs of the electrodes, two main differences were observed. First, both the anodic and cathodic peak potentials shift with different preparation methods

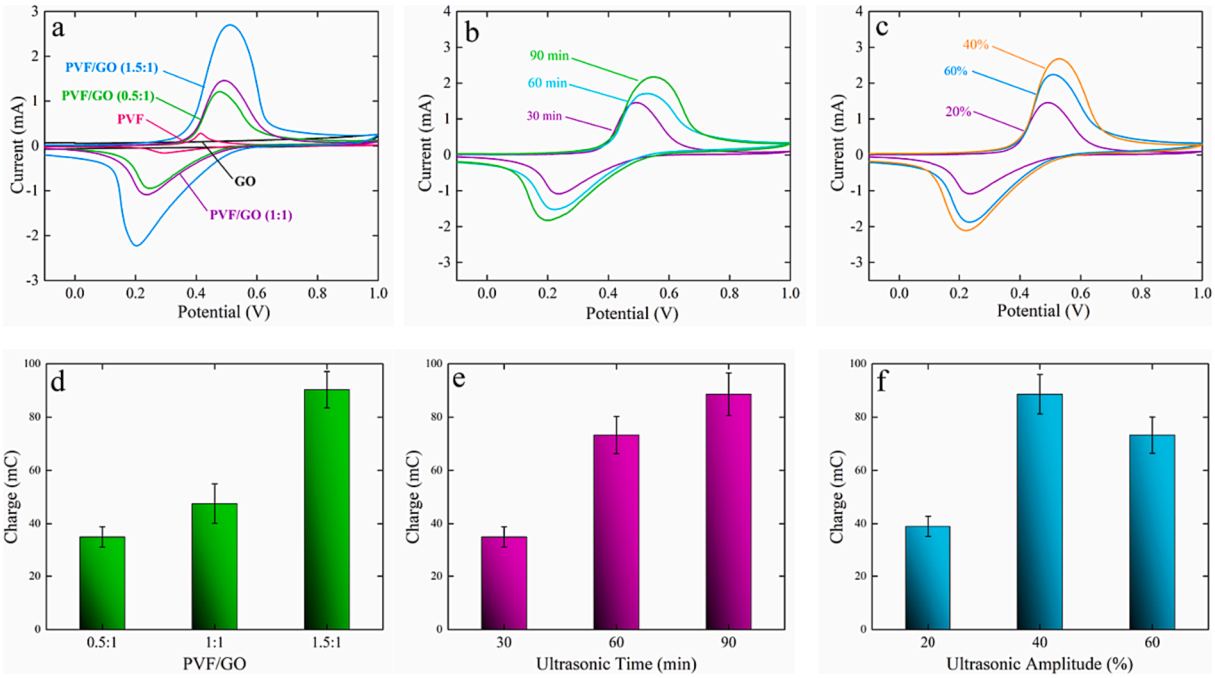

Fig. 2. Cyclic voltammograms comparison of the PVF/GO electrodes prepared at different (a) PVF/GO ratio, (b) sonication time, and (c) ultrasonic amplitude under Ar in 0.1 M $LiClO_4$ at the scan rate of 5 mV/s. Electrochemical charge comparison of the PVF/GO electrodes prepared at different (d) PVF/GO ratio (0.5:1, 1:1, 1.5:1), (e) sonication time (30, 60, 90 min), and (f) ultrasonic amplitude (20, 40, 60%).

and the ink compositions. Thereby, the peak potentials of each electrode also change, having an effect on the electrochemical reversibility of the redox reaction. As peak differences increase, the rate of electron transfer decreases. Given this information, it is clear that the rate of electron transfer can vary between the electrodes used. Second, variations in the peak areas for both the anodic and the cathodic peaks were identified, which indicates that the ink composition and preparation method has a significant impact on the performance of electrode.

As stated in the literature [43,44], the reaction mechanism at the anode can be written as below.

$$Fc - e^- + A^- \rightleftarrows Fc^+A^-$$

where Fc and Fc^+ show the reduced and oxidized states of the redox active center, respectively, and A indicates the anion in the aqueous solution. Following the oxidation of the anode, the uncharged reduced state ferrocene is oxidized to the ferrocenium and has a net positive charge which subsequently leads to adsorption of anions from the solution. In addition to electrostatic attraction, hydrogen bonding also plays a role in regulating the strength of the adsorption force.

Formate is selectively adsorbable from the solution when ferrocene units on the electrode surface are oxidized. As previously mentioned, the number of active surface sites on the electrode can be determined from the area under the anodic peak, and the highest performing electrode can be identified by comparing the area under the anodic peaks of each. In other words, there is a direct correlation between the number of oxidized ferrocene units and the area under the anodic peak and the number of active surface sites that adsorb formate. Oxidation of ferrocene units creates a pass-through charge, and the measured charge from CV peaks is proportional to the amount of PVF deposited. As can be seen in Fig. 2, the co-deposited electrode prepared using a 1.5:1 PVF/GO ratio had the highest charge of 90.3 ± 6.8 mC, which indicates that it had a larger adsorption capacity than the electrodes prepared with a lower PVF/GO ratio. In addition, the quantity of oxidized ferrocene units on the electrode surface varied significantly with how the PVF/GO dispersion had been prepared. The electrode prepared with an ultrasonic amplitude of 40% had a clearly higher charge value than those of 20 and 60%. An initial increase in the charge was observed for the ultrasonic amplitude at 40%, but dropped when this charge was increased to 60%. Finally, the electrode prepared with a sonication time of 30 min had a lower charge value (35.0 ± 3.7 mC) than those prepared with sonication times of 60 min (73.3 ± 7.0 mC) and 90 min (88.6 ± 8.1 mC).

To better characterize the constructed electrodes, the morphological properties of the prepared PVF/GO electrodes were investigated using scanning electron microscopy (SEM). The SEM image in Fig. 3a shows that the surface of CP consists of uniform fibers with long and compact structures and a smooth surface, which is in good agreement with the literature [45–47]. The average diameter of the fibers estimated from the images is ~ 10 μm. The CP electrode treated by electrochemical oxidation in the PVF/DMF dispersion indicates non-homogenous and irregular polymer layers formed on the electrode surface and partially covering the empty spaces between carbon fibers (Fig. 3b). This was anticipated because the polymer turned solvophobic once it was oxidized and transferred to the electrode's surface. CV measurements further supported the identification of PVF on the electrode surface. When the electrode surface (Fig. 3c) was coated with only a dispersion with GO/DMF was examined, it was observed that the surface had a morphology similar to that of the untreated CP. That is, use of only GO/DMF had nearly no effect on the coating of the CP surface.

The SEM images in Fig. 3d–f show the effect of different PVF/GO ratios on electrode morphology. With the increase in the PVF/GO ratio from 0.5 to 1.5, coating amounts on the electrode surface increased. Under conditions in which the PVF/GO ratio was 0.5, the coating efficiency and quality were somewhat low. Agglomeration tendency was observed on the electrode surface at all three PVF/GO ratios, albeit at a low level. The SEM images (Fig. 3g–i) show the effect of ultrasonic time on the CP electrode morphology at a PVF/GO ratio of 1.0 and 20% ultrasonic amplitude. Increasing the ultrasonic time from 30 to 60 min caused agglomeration tendency to considerably increase and decreased the coating quality of the surface. A significant agglomeration tendency was not observed at 90 min. The SEM images in Fig. 3j–l show the effect of ultrasonic amplitude on electrode morphology at a PVF/GO ratio of 0.5 and 30 min ultrasonic time. As can be seen, ultrasonic amplitude had a remarkable effect on electrode morphology. Particularly under high

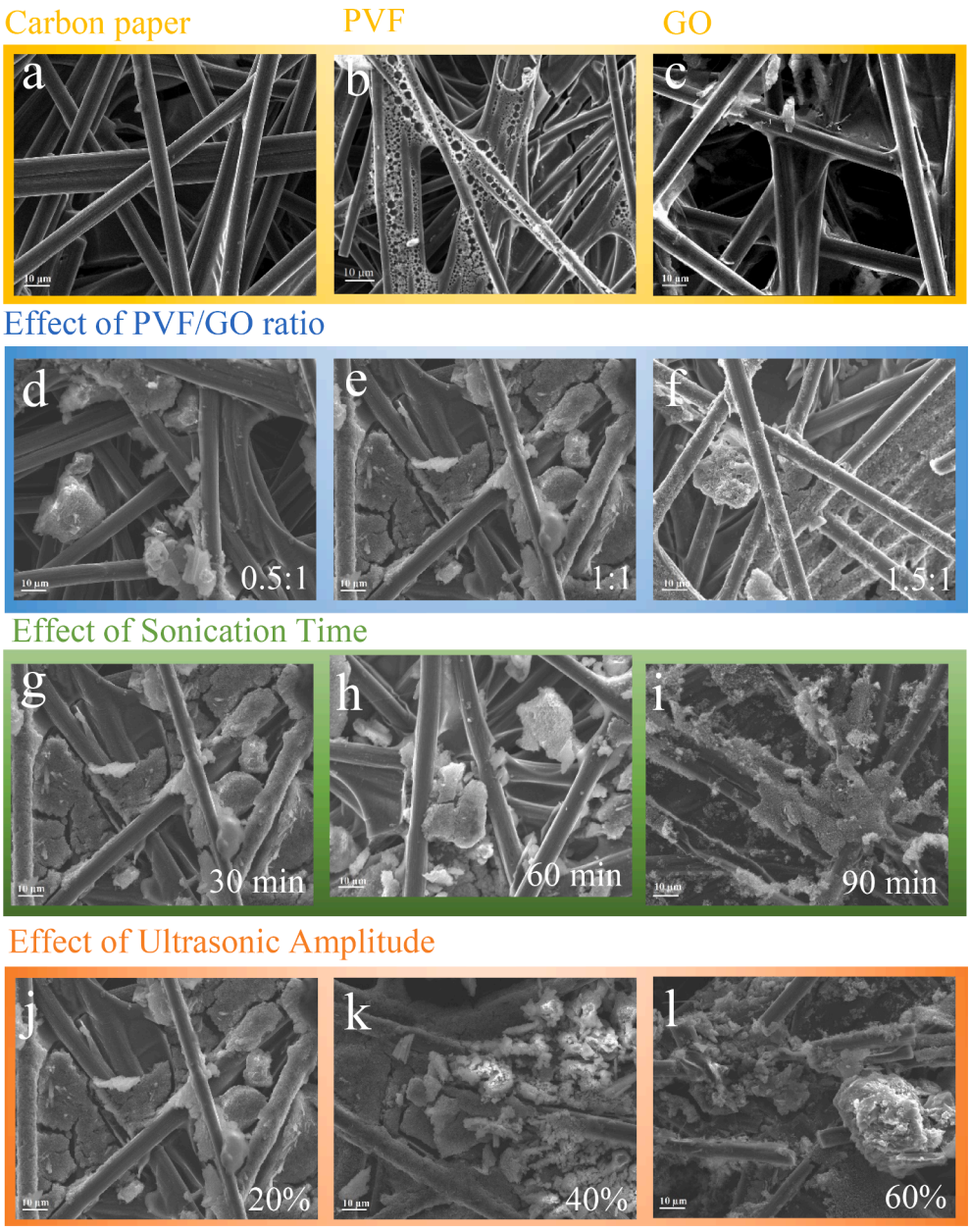

Fig. 3. Scanning electron microscopy (SEM) images of (a) untreated carbon paper electrode, (b) carbon paper electrode treated by electrochemical oxidation in the PVF/DMF dispersion, and (c) GO/DMF dispersion. Effect of PVF/GO ratio on the surface morphology of the electrodes obtained treated by electrochemical oxidation. SEM images of the electrodes fabricated at different PVF/GO values (d) 0.5:1, (e) 1:1, and (f) 1.5:1. Effects of different ultrasonic treatments on the surface morphology of the PVF/GO electrodes obtained treated by electrochemical oxidation. SEM images of the electrodes exposed for (g) 30 min, (h) 60 min, and (i) 90 min ultrasonic time at PVF/GO 1 and 20% ultrasonic amplitude; (j) 20%, (k) 40%, (l) 60% ultrasonic amplitude at PVF/GO 1 and 30 min ultrasonic time.

amplitude conditions (e.g., 60%), intense agglomeration tendencies as well as major deformations on the electrode surfaces were observed. Further evaluation shows that the electrode morphology was more homogenously coated at 40% ultrasonic amplitude. In this case, a more stable film was created and dispersed on the substrate by the π–π interaction between ferrocene moieties and GOs.

When the results of electrochemical and morphological analyses were evaluated together, each of the three parameters had a different effect on electrode performance. For example, although increasing the PVF/GO ratio positively affected electrode performance, increasing the ultrasonic amplitude had the inverse effect and decreased the performance. In addition, the electrochemical performance of the electrode and the subsequent efficiency of formate adsorption were greatly influenced by the proper coating of the electrode surfaces. This specific experimental design technique was used to gain a deeper understanding of the PVF/GO ratio, ultrasonic amplitude, and time effects over the prepared electrodes.

3.2. Experimental design results

In the present study, the effect of the PVF/GO ratio, sonication time, and ultrasonic amplitude on the number of active surface sites and the efficiency of formate adsorption was investigated using the three-variable Box–Behnken experimental design. Furthermore, it was used to determine the significance of individual parameters and the combined interaction effects of the parameters on both responses. Based on these results, the relationship between the independent variables and the predicted responses in terms of coded factors for both the number of active sites (NAS) and the adsorption efficiency (AE) was formulated in Eqs. (6) and (7).

$$Y_{NAS} = 86.67 + 23.04A + 6.09B + 4.15C + 2.25AB - 2.83AC - 1.43BC - 15.03A^2 - 6.98B^2 - 11.36C^2 \quad (6)$$

$$Y_{AE} = 79.70 + 21.92A + 7.49B + 4.96C + 1.05AB - 4.50AC - 2.88BC - 15.59A^2 - 8.81B^2 - 12.61C^2 \quad (7)$$

The values and signs of coded coefficients indicate the significance level on the number of active surface sites and the adsorption efficiency. The positive sign in these second-order polynomial equations indicates the synergistic and favorable effect of the output response. Looking at Eqs. (6) and (7), the PVF/GO ratio with the largest coded coefficient imposed the most significant effect on both responses, while the simultaneous effect of a combination of sonication time and ultrasonic amplitude showed the least significance level in this model. Because the coefficients of the PVF/GO ratio, sonication time, and ultrasonic amplitude were positive, the adsorption efficiency increased with an increase in these parameters.

Analysis of variance (ANOVA) was used to evaluate the significance of the quadratic models and identify the terms that had the most impact on both responses, and the detailed ANOVA results are shown in Tables S2 and S3. According to ANOVA, a larger value of F and a smaller value of p (i.e., $p < 0.05$) demonstrated that the model is statistically significant. The F-test gave a low probability value, which also indicated the high significance of the model for both responses. Moreover, the model determination coefficient, R^2, of 0.9713 and 0.9709 for the number of active surface sites and formate adsorption efficiency further showed a good correlation between the measured and predicted responses. Based on the obtained p-value, the PVF/GO ratio was observed to be the most significant factor that affected the efficiency of formate adsorption with the least p-value compared to the other two parameters, with a P-value of < 0.0001. In addition, both sonication time and the ultrasonic amplitude had a significant impact on adsorption efficiency; however, the interaction between each of the three parameters showed insignificant effects with $p > 0.1$. The quadratic terms affected the number of active surface sites and formate adsorption efficiency in the following order: $A^2 > C^2 > B^2$.

The predicted values were close to the observed experimental values (Fig. 4a, b), which meant that Box–Behnken design was suitable for both responses. The perturbation plots used to examine the simultaneous effect on formate adsorption efficiency of the three factors are seen in Fig. 4c–d. Formate adsorption efficiency was determined using this plot as observed when each variable moved from a reference point; no other factors were involved. Hence, this perturbation plot shows a deviation from the adjusted reference point using variables, which ranged from −1 to + 1 on the abscissa. This indicated the coded value and the ordinate standard of formate adsorption efficiency using just one factor. The sharp curvature observed for each variable shows a significant effect on the maximum formate adsorption efficiency; however, there was a difference in positive and negative deviations and their effects on adsorption efficiency. When the effects of sonication time and ultrasonic amplitude were examined and the deviations ranged from −1 to + 1, there was an initial increase and then a decrease in formate adsorption efficiency.

Using RSM, the effects of the independent variables on the number of active surface site and formate adsorption efficiency were plotted in three-dimensional (3D) response surface plots and two-D (2D) contour plots and the results are given in Figs. S2 and S3. The main aim of the response surface is to monitor variables efficiently for the optimum values to maximize the response. The best response range can be calculated by analyzing the plots. Based on these 3D and 2D plots together, it can be concluded that increasing the PVF/GO ratio and ultrasonic time resulted in an increased both the active surface cite and adsorption efficiency. As the applied ultrasonic amplitude increased, a significant decrease in adsorption efficiency was observed.

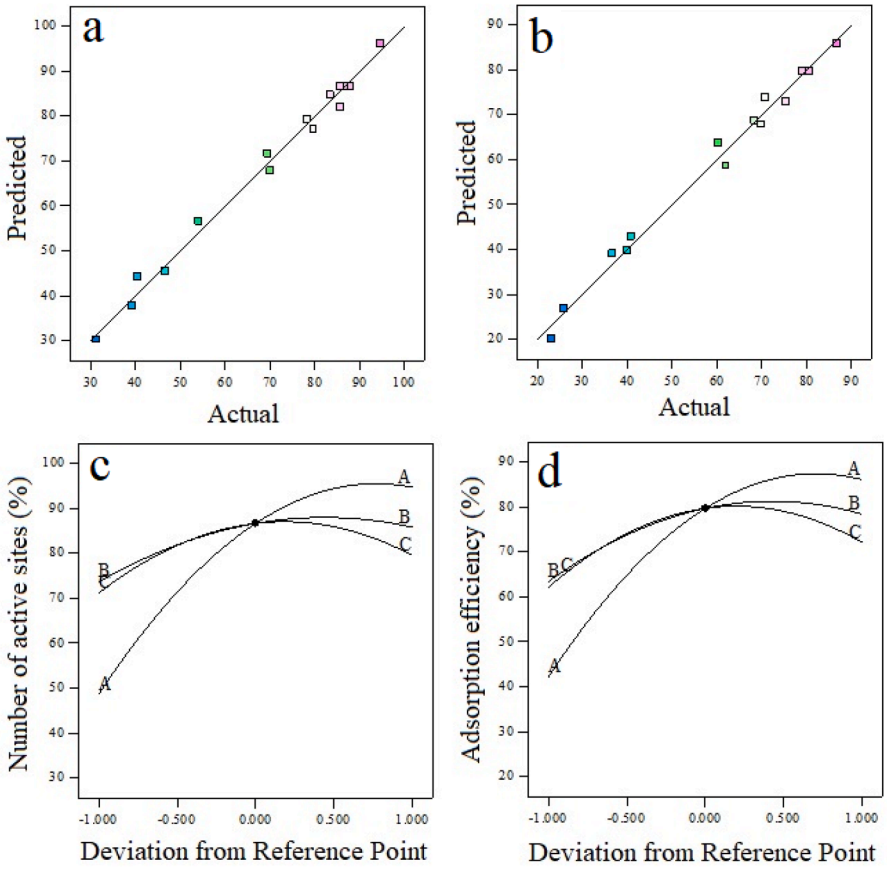

Fig. 4. Plot of the predicted response versus observed response for (a) the number of active surface sites (%), and (b) formate adsorption efficiency (%). The perturbation plot of each factor (A: PVF/GO ratio, B: sonication time, and C: ultrasonic amplitude) for (c) the number of active surface sites (%), and (d) formate adsorption efficiency (%).

3.3. Flow system results

After fabrication and characterization of the PVF/GO electrodes at the small scale (1 × 2 cm), the performance of the electrochemical cell was tested under realistic conditions at constant voltage and continuous-flow of a supporting lithium perchlorate electrolyte in the absence of formate ions. This study was the first to implement PVF/GO-based electrodes in a flow-cell system to achieve formate separation. During this process, a voltage was imposed across two symmetric PVF/GO electrodes that induced the adsorption of anions at the anode and cations at the cathode. The flow-cell performance was evaluated based on batch-mode experiments conducted using symmetric electrodes in a custom-made electrochemical cell. There were three steps used for this basic operation as follows: (1) uncharged, (2) adsorption/charging, and (3) desorption/discharging. Before beginning the experiments, the cell was flushed with deionized water, after which 10 mM $LiClO_4$ solution was allowed to pass through the cell at a constant flow rate of 0.5 mL/min to initiate the electrochemical separation. During the uncharged step, redox-active moieties were found on the anode and cathode after connecting the electrodes to the power source at a charging rate of 1 V for 5 min for adsorption and a discharge rate of −1 V for 5 min for desorption. During the experiment, this cycle was repeated for five successive runs to ensure that a dynamic steady state was provided. Electrochemical measurements involved stepping the voltage between the electrodes 1.0 V for 5 min, and with a net positive charge, the redox moieties on the anode were oxidized to ferrocenium. The charge that was applied led to anion adsorption from the influent through hydrogen bonding and electrostatic attraction to control the strength of the adsorption process [44]. When the potential was applied and ions were electrostatically adsorbed onto the electrodes, the electrodes became saturated and needed to be regenerated. After this charging phase, the applied potential was removed and the electrodes regenerated by setting the voltage difference to −1.0 V, applying a reverse potential. The applied voltage step and current response are illustrated in Fig. 5a. During the charging step, the measured current initially peaked but then quickly declined. Immediately after the voltage changed, the driving force for electrosorption was maximized, and a substantial quantity of anions from the electrolyte were adsorbed, which resulted in a peak current. The current deteriorated rapidly over time as more and more saturation with adsorbed species was observed on the surface. After charging for 5 min, the electrostatic potential that was applied was adjusted to −1.0 V, and an inverted current response was observed. The ionic charge that was accumulated in the electrode was allowed to escape the electrode, which then led to the release of the adsorbed ions

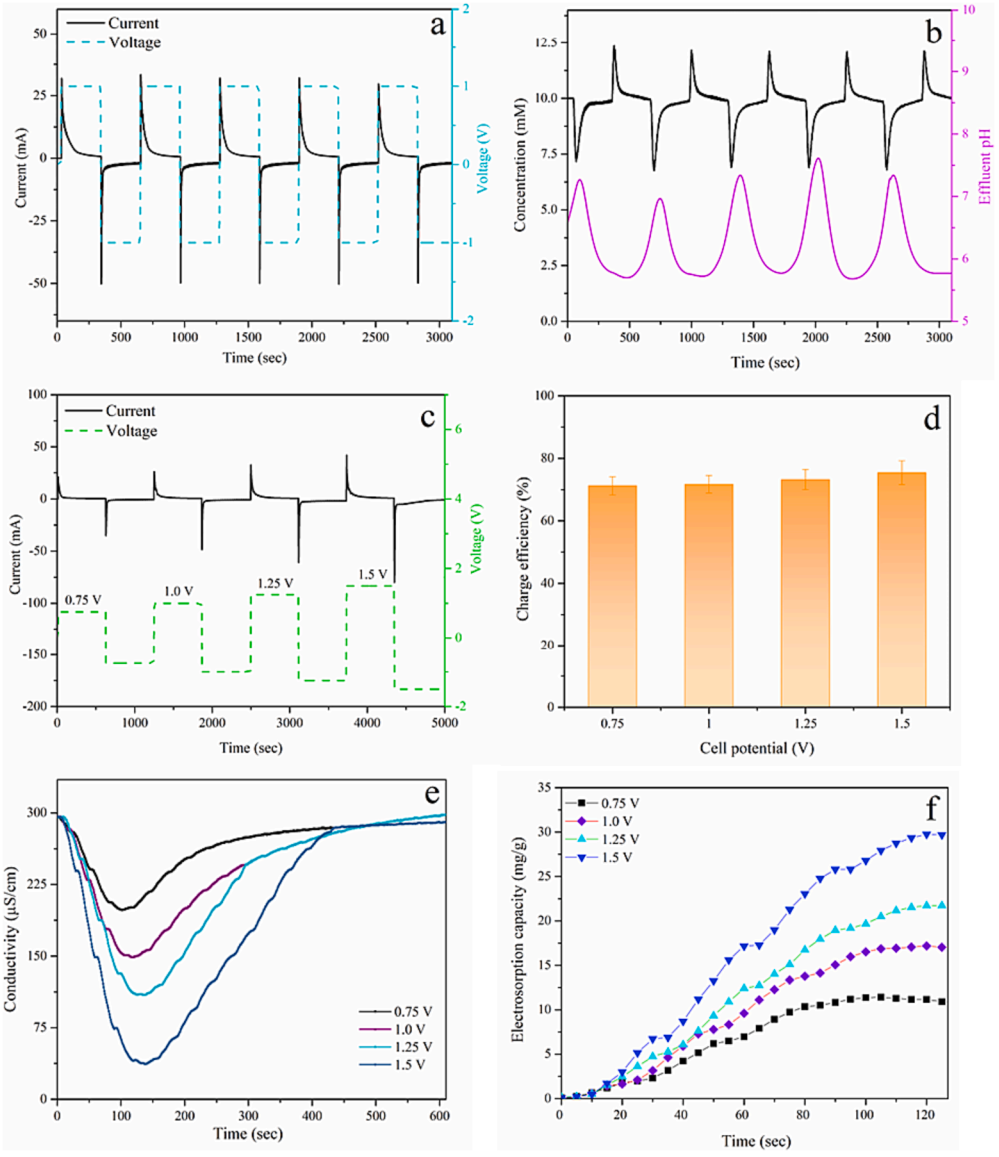

Fig. 5. Cycling performance of symmetric redox-active electrode pair under charging at 1.0 V and discharging at −1.0 V cell voltage in 10 mM $LiClO_4$ electrolyte solution. (a) Current and voltage profiles and (b) the effluent concentration and pH of perchlorate ions. Cycling performance of symmetric redox-active electrode pair under different charging and discharging cell voltage in 10 mM $LiClO_4$ electrolyte solution. (c) Current and voltage profiles and, (d) the charge efficiencies with respect to applied potential. (e) Electrosorption of PVF/GO electrodes in 10 mM $LiClO_4$ electrolyte solution under different applied voltages, and (f) corresponding electrosorption capacities against applied potential.

back into solution. The effluent's conductivity and pH were continuously recorded during the experiments to monitor the cell's performance. Fig. 5b shows the effluent concentration and pH of the perchlorate ions, which exhibit typical adsorption/desorption behavior. When the voltage was applied, there was a net drop in electrolyte concentration, which was concurrent with a sharp increase in the measured current because of ion adsorption. The charged ions were then drawn to the opposite electrodes and stored. After the deionized solution passed through and exited the cell, its conductivity was measured. As the electrodes became saturated over time, the concentration of the solution gradually increased until it nearly reached its initial value. A sharp increase in concentration was also observed during the discharge step as the adsorbed ions were desorbed into the electrolyte. The high concentration that was initially recorded gradually decreased to near the initial concentration (Fig. 5b). That is, as the electrodes regenerated, a sharp increase in concentration was observed as all the adsorbed ions were released from the electrodes. Over time, as the electrodes were again fully regenerated, the concentration returned to its initial value. In addition, the five adsorption/desorption cycles behaved similarly, which indicated that a dynamic steady state had been reached. Fig. S4 shows the prolonged cycling performance of the PVF/GO electrodes and the profile kept stable after 2 h of cycling, demonstrating the high reversibility of the electrodes. The pH varied between 5.7 and 7.6 during the experimental process. During the adsorption stage, pH increased; during the desorption stage, it decreased.

Experiments were also conducted at potentials ranging from 0.75 to 1.50 V in 10 mM $LiClO_4$ electrolyte solution at a constant flow rate of 0.5 mL/min. Fig. 5c and 5d show these profiles and their charge efficiencies. As clearly seen in Fig. 5c, a larger applied voltage increased the current and provided larger charge efficiency of the flow cell. The charge efficiency at 1.5 V caused the electrochemical cell to reach the highest value of 75.4 ± 3.8%. Fig. 5e shows the conductivity transition at 0.75, 1.0, 1.25, and 1.5 mV, which indicated that higher voltages were favorable for electrosorption because the resulting electric field was stronger. In addition, the increased voltage enabled a more rapid rate of electrosorption, with the highest capacity of 29.68 mg/g occurring at 1.5 V—a significant improvement from the result of the lower voltage.

In the present study, in addition to a low flow rate (0.5 mL/min), the electrochemical cell was operated using higher flow rate values considering the scale-up technology. The experiments were conducted at 5.0 mL/min. The results are provided in Fig. S5. The total cycle charge efficiency was calculated to indicate the performance of the flow process. It can be concluded that the charge efficiency increased by decreasing the flow rate and vice versa. The calculated charge efficiency at 0.5 mL/s was 17% higher than that at 5.0 mL/s.

3.4. Selective formate recovery in flow-cell system

Thanks to the prepared PVF/GO redox-active electrodes, anions can adsorb at the anode and cations at the cathode. The electrodes demonstrated ion adsorption behavior during the charge step and released the ions to solution during the discharge step when paired and tested for applications of selective separation of ions. The process exhibited strong electrosorption behavior when cell operations alternated between adsorption and desorption modes. In addition, the results indicated that the total cycle charge efficiency of the process was > 75% under studied operating conditions. After the flow-cell system was tested and optimized, the formate ions were selectively separated under specific flow conditions. The flow system provided a more realistic assessment of dynamic selectivity using charging and discharging instead of a single equilibrium adsorption step (Fig. 6).

As stated in one study [44], hydrogen bonds form between a charged conduction polymer (i.e., ferrocenium) and anions, which is the result of groups from which electrons are withdrawn. This bond is much stronger than those from electrostatic interactions with anions. Formate removal was quantified using a background electrolyte. A feed solution

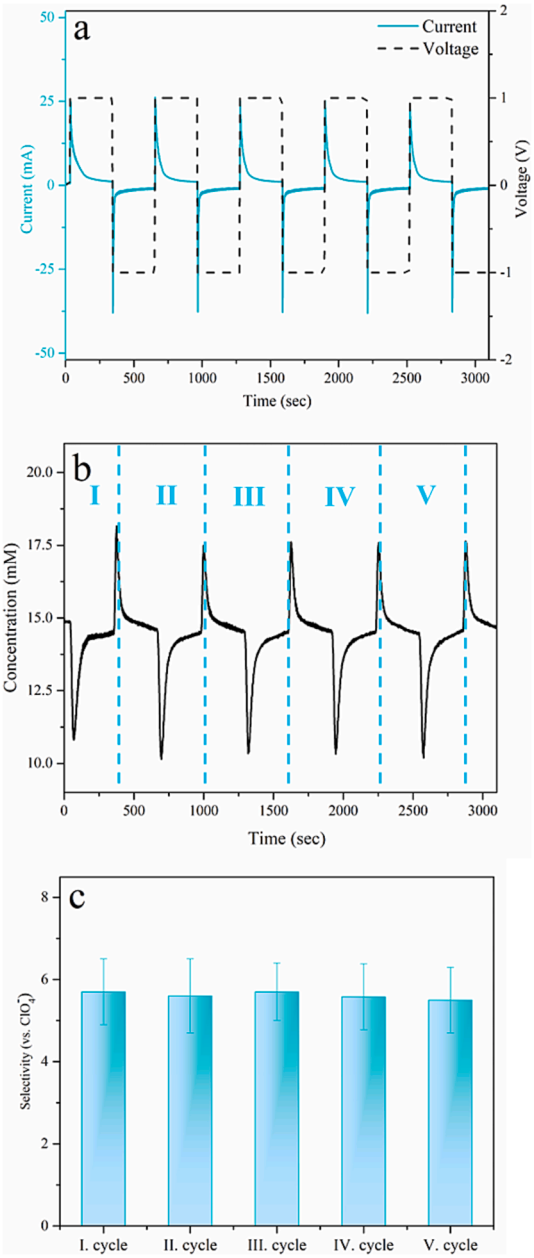

Fig. 6. Selective removal of formate from aqueous solution in the presence of perchlorate ions using PVF/GO redox-active electrodes. (a) Current and voltage profiles and (b) the effluent concentration under charging at 1.0 V and discharging at −1.0 V cell voltage in 0.5 mM formate and 15 mM $LiClO_4$ electrolyte. (c) Calculated selectivity of formate ions with respect to perchlorate ions (in 30-fold abundance) for each cycle.

containing 0.5 mM formate and 15 mM $LiClO_4$ (30:1) was used to evaluate formate selectivity as it related to the background anion, which was 0.5 mM formate as the target anion and at 15 mM perchlorate as the competing anion. HPLC was used to measure formate concentration with aliquots of 100 μL from the effluent after every cycle. We calculated the selectivity of formate ions against the perchlorate ions as follows:

$$S_{formate} = \frac{(\Delta C/C_0)_{formate}}{(\Delta C/C_0)_{perchlorate}} \quad (8)$$

where C_0 is the initial concentration (0.5 mM here) and ΔC is the change in concentration after a given time. Under flow conditions at 30-fold supporting anions, cycle selectivity was 5.7 ± 0.8 for first cycle. The

selectivity of each cycle was very similar to each other. The rapid adsorption of the perchlorate ions and stabilization of the ferrocenium moieties on the electrode surface were observed because of the significant excess of this anion in comparison to the formate. On the other hand, over time, the formate, which was more dilute, started to be adsorbed onto the electrode surface. As it also had a higher binding strength with ferrocenium than perchlorate did, it replaced the perchlorate anion, and as a result, the ratio of adsorbed formate relative to perchlorate became 5.7 times higher than their ratio inside the feed stream. In addition to selectivity, one of the interesting qualities of redox electrodes is the reversibility of adsorption and the recovery of adsorbed compounds. This reversibility was tested with desorption experiments and the efficiency of formate ion recovery was determined as 80.7 ± 3.1%. In addition, we calculated the volumetric energy consumption (E_v) for evaluating the economic separation performance of the system, and this value was 0.088 kWh/m^3.

The SEM images of the PVF/GO electrodes obtained at uncharged, charging, and discharging steps within the flow-cell system are shown in Fig. S6. When the SEM image of the PVF/GO electrodes after formate adsorption process is examined, the formate ions were homogenously adsorbed onto the surface and the voids are nearly filled; however, as a result of the desorption process, irregular holes were occurred on the PVF/GO electrode surface.

3.5. Application results

In the present study, after ensuring that the electrochemical cell worked well under flow conditions, the selective separation of formate ions was investigated using the solution obtained in the CO_2 electrolysis processes to simulate more realistic conditions. In an electrolyzer, CO_2 is reduced on the cathode while the oxygen evolution reaction occurs on the anode. Here, the CO_2 reduction reaction was conducted at different potentials in a CO_2 saturated 0.1 M $KHCO_3$ electrolyte using a glass H-type cell. A Nafion 117 cation exchange membrane was used as a separator to avoid oxidation of CO_2 reduction products. After 1 h of electrolysis, a liquid sample was collected. This liquid samples contained the products formed as a result of the electrochemical reduction of CO_2 in 0.1 M saturated $KHCO_3$ electrolyte at different potentials. First, the initial content of the solution was determined using HPLC (Fig. S7). When the results were examined, the concentration of the formate ion was 1% of the electrolyte solution used. In addition, methanol, ethanol, and small amount of acetaldehyde were detected in the solution, which was expected. The same voltage values were applied to the cell for the adsorption (1.0 V for 5 min) and desorption (-1.0 V for 5 min) steps under a single pass flow of 0.5 mL/min for five consecutive cycles. At the end of each adsorption and desorption step, the effluent was stored in two separate containers. First, the cell was fed with 10 mM $LiClO_4$ electrolyte at a constant flow rate of 0.5 mL/min. During the adsorption process, the formate ions were adsorbed on the electrode surface, the output stream contained less ions, and collected in the first container. The recovery of the adsorbed formate ions was achieved by applying a more negative potential to the working electrode to reduce the ferrocenium and thus release the adsorbed formate ions to the electrolyte. When a negative voltage was applied to the system, the formate ion accumulated on the PVF/GO electrode surface was desorbed and this output stream, which was more concentrated in formate ion, was collected in the second container. After six consecutive cycles, i.e., 1 h later, we were able to obtain a 5.8 times more concentrated formate solution compared to feed solution. Our experimental results also show that when the concentrated formate solution was fed back to the electrochemical cell as a feed stream, a 16.8 times more concentrated formate solution was obtained at 72 h compared to a 1% starting solution. In addition, the results showed selectivity of > 4.0 toward formate compared to a liquid product, including the bicarbonate electrolyte in 100-fold abundance. This technology as demonstrated would require that the electrodes remain stable over several adsorption/desorption cycles and the use of high active material loading and large electrode areas to achieve capacity high enough for industrial applications.

4. Conclusion

In the present study, the selective separation process of formate ions was demonstrated in a continuous-flow process. First, PVF/GO electrodes were fabricated using the drop-casted method and characterized electrochemically and morphologically. The effect of the PVF/GO ratio, sonication time, and ultrasonic amplitude on the number of active surface sites on the electrode and the formate adsorption efficiency were investigated using the Box–Behnken experimental design technique. The results revealed that, among the three examined, the PVF/GO ratio was the most significant factor that affected the responses. It was observed that the second-order polynomial model was sufficient to accurately predict the effect of the parameters on adsorption efficiency. The optimum conditions were identified as 1.5 PVF/GO ratio, 90 min sonication time, and 40% ultrasonic amplitude within the tested range, and the adsorption efficiency reached $> 85\%$. The flow-platform was then established for large-scale formate separation and that used the PVF/GO electrodes fabricated under optimization conditions. Our results indicated that formate, the organic ion, was selectively removed at a 5.7-fold rate against a 30-fold abundance of perchlorate-supporting anion. The performance of the flow cell was also tested using a solution that contained different liquid CO_2 reduction products. Here a product stream containing more concentrated formate could be obtained due to selective formate separation in the flow cell. This clearly indicates that electrochemically mediated adsorption in a continuous-flow process has a potential use for selective formate separation on a larger scale.

CRediT authorship contribution statement

Sevgi Polat: Conceptualization, Methodology, Investigation, Visualization, Writing – original draft, Writing – review & editing. **Ruud Kortlever:** Conceptualization, Supervision, Writing – review & editing. **Hüseyin Burak Eral:** Conceptualization, Supervision, Writing – review & editing.

Declaration of Competing Interest

The authors declare that they have no known competing financial interests or personal relationships that could have appeared to influence the work reported in this paper.

Data availability

Data will be made available on request.

Acknowledgements

S. Polat would like to acknowledge financial support from the Scientific and Technological Research Council of Turkey (TUBITAK 2219) [Grant No: 1059B192000847]. The authors thank Dr. Ahmed Mohsen Ismail for providing the solution obtained in the CO_2 electrolysis processes.

Appendix A. Supplementary data

Supplementary data to this article can be found online at https://doi.org/10.1016/j.cej.2023.146169.

References

[1] J. Hansen, M. Sato, R. Ruedy, K. Lo, D.W. Lea, M. Medina-Elizade, Global temperature change, Proc. Natl. Acad. Sci. U. S. A. 103 (2006) 14288–14293, https://doi.org/10.1073/pnas.0606291103.

[2] V. Ramanathan, Y. Feng, Air pollution, greenhouse gases and climate change: Global and regional perspectives, Atmos. Environ. 43 (2009) 37–50, https://doi.org/10.1016/j.atmosenv.2008.09.063.

[3] M. New, Preface: Four degrees and beyond: The potential for a global temperature increase of four degrees and its implications, Philos. Trans. R. Soc. A Math. Phys. Eng. Sci. 369 (2011) 4–5, https://doi.org/10.1098/rsta.2010.0304.

[4] S.J. Davis, K. Caldeira, H.D. Matthews, Future CO2 emissions and climate change from existing energy infrastructure, Science (80-.) 329 (2010) 1330–1333, https://doi.org/10.1126/science.1188566.

[5] L.C. Lau, K.T. Lee, A.R. Mohamed, Global warming mitigation and renewable energy policy development from the Kyoto Protocol to the Copenhagen Accord - A comment, Renew. Sustain. Energy Rev. 16 (2012) 5280–5284, https://doi.org/10.1016/j.rser.2012.04.006.

[6] H. Yoon, J. Lee, S. Kim, J. Yoon, Review of concepts and applications of electrochemical ion separation (EIONS) process, Sep. Purif. Technol. 215 (2019) 190–207, https://doi.org/10.1016/j.seppur.2018.12.071.

[7] D. Johnson, Z. Qiao, A. Djire, Progress and Challenges of Carbon Dioxide Reduction Reaction on Transition Metal Based Electrocatalysts, ACS Appl. Energy Mater. 4 (2021) 8661–8684, https://doi.org/10.1021/acsaem.1c01624.

[8] C. Song, CO2 Conversion and Utilization: An Overview, ACS Symp. Ser. 809 (2002) 1–30, https://doi.org/10.1021/bk-2002-0809.ch001.

[9] D. Ewis, M. Arsalan, M. Khaled, D. Pant, M.M. Ba-Abbad, A. Amhamed, M.H. El-Naas, Electrochemical reduction of CO2 into formate/formic acid: A review of cell design and operation, Sep. Purif. Technol. 316 (2023), 123811, https://doi.org/10.1016/j.seppur.2023.123811.

[10] S. Roy, A. Cherevotan, S.C. Peter, Thermochemical CO2 Hydrogenation to Single Carbon Products: Scientific and Technological Challenges, ACS Energy Lett. 3 (2018) 1938–1966, https://doi.org/10.1021/acsenergylett.8b00740.

[11] S.C. Peter, Reduction of CO2 to Chemicals and Fuels: A Solution to Global Warming and Energy Crisis, ACS Energy Lett. 3 (2018) 1557–1561, https://doi.org/10.1021/acsenergylett.8b00878.

[12] A. Tripathi, R. Thapa, Optimizing CO2RR selectivity on single atom catalysts using graphical construction and identification of energy descriptor, Carbon N. Y. 208 (2023) 330–337, https://doi.org/10.1016/j.carbon.2023.03.065.

[13] X. An, P. Wang, X. Ma, X. Du, X. Hao, Z. Yang, G. Guan, Application of ionic liquids in CO2 capture and electrochemical reduction: A review, Carbon Resour. Convers. 6 (2023) 85–97, https://doi.org/10.1016/j.crcon.2023.02.003.

[14] F. Yang, H. Yu, X. Mao, Q. Meng, S. Chen, Q. Deng, Z. Zeng, J. Wang, S. Deng, Boosting electrochemical CO2 reduction on ternary heteroatoms-doped porous carbon, Chem. Eng. J. 425 (2021), 131661, https://doi.org/10.1016/j.cej.2021.131661.

[15] G.Z.S. Ling, J.J. Foo, X.Q. Tan, W.J. Ong, Transition into Net-Zero Carbon Community from Fossil Fuels: Life Cycle Assessment of Light-Driven CO2 Conversion to Methanol Using Graphitic Carbon Nitride, ACS Sustain. Chem. Eng. (2022), https://doi.org/10.1021/acssuschemeng.2c07375.

[16] J. Vehrenberg, J. Baessler, A. Decker, R. Keller, Paired Electrochemical Synthesis of Formate via Oxidation of Glycerol and Reduction of CO2 in a Flow Cell Reactor, Electrochem. Commun. (2023), 107497, https://doi.org/10.1016/j.elecom.2023.107497.

[17] K. Armstrong, P. Styring, Assessing the potential of utilization and storage strategies for post-combustion CO 2 emissions reduction, Front. Energy Res. 3 (2015) 1–9, https://doi.org/10.3389/fenrg.2015.00008.

[18] A. Taheri Najafabadi, CO2 chemical conversion to useful products: An engineering insight to the latest advances toward sustainability, Int. J. Energy Res. 37 (2013) 485–499, https://doi.org/10.1002/er.3021.

[19] C. Xia, P. Zhu, Q. Jiang, Y. Pan, W. Liang, E. Stavitsk, H.N. Alshareef, H. Wang, Continuous production of pure liquid fuel solutions via electrocatalytic CO2 reduction using solid-electrolyte devices, Nat. Energy 4 (2019) 776–785, https://doi.org/10.1038/s41560-019-0451-x.

[20] L. Fan, C. Xia, F. Yang, J. Wang, H. Wang, Y. Lu, Strategies in catalysts and electrolyzer design for electrochemical CO2 reduction toward C2+ products, Sci. Adv. 6 (2020) 1–18, https://doi.org/10.1126/sciadv.aay3111.

[21] R. Kortlever, J. Shen, K.J.P. Schouten, F. Calle-Vallejo, M.T.M. Koper, Catalysts and Reaction Pathways for the Electrochemical Reduction of Carbon Dioxide, J. Phys. Chem. Lett. 6 (2015) 4073–4082, https://doi.org/10.1021/acs.jpclett.5b01559.

[22] M.N. Hossain, R.M. Choueiri, S. Abner, L.D. Chen, A. Chen, Electrochemical Reduction of Carbon Dioxide at TiO2/Au Nanocomposites, ACS Appl. Mater. Interfaces 14 (2022) 51889–51899, https://doi.org/10.1021/acsami.2c14368.

[23] K. Fernández-Caso, G. Díaz-Sainz, M. Alvarez-Guerra, A. Irabien, Electroreduction of CO2: Advances in the Continuous Production of Formic Acid and Formate, ACS Energy Lett. 8 (2023) 1992–2024, https://doi.org/10.1021/acsenergylett.3c00489.

[24] H. Yuan, Z. Liu, S. Sang, X. Wang, Dynamic re-construction of sulfur tailored Cu2O for efficient electrochemical CO2 reduction to formate over a wide potential window, Appl. Surf. Sci. 613 (2023), 156130, https://doi.org/10.1016/j.apsusc.2022.156130.

[25] X. An, S. Li, Z. Yang, X. Ma, X. Hao, A. Abudula, G. Guan, F-doped In(OH)3 for electrochemical reduction of CO2 to formate, Chem. Eng. J. 455 (2023), 140720, https://doi.org/10.1016/j.cej.2022.140720.

[26] L. Fan, C. Xia, P. Zhu, Y. Lu, H. Wang, Electrochemical CO2 reduction to high-concentration pure formic acid solutions in an all-solid-state reactor, Nat. Commun. 11 (2020) 1–9, https://doi.org/10.1038/s41467-020-17403-1.

[27] M. Ramdin, A.R.T. Morrison, M. De Groen, R. Van Haperen, R. De Kler, E. Irtem, A. T. Laitinen, L.J.P. Van Den Broeke, T. Breugelmans, J.P.M. Trusler, W. De Jong, T. J.H. Vlugt, High-Pressure Electrochemical Reduction of CO2 to Formic Acid/Formate: Effect of pH on the Downstream Separation Process and Economics, Ind. Eng. Chem. Res. 58 (2019) 22718–22740, https://doi.org/10.1021/acs.iecr.9b03970.

[28] B.S. Jayathilake, S. Bhattacharya, N. Vaidehi, S.R. Narayanan, Efficient and Selective Electrochemically Driven Enzyme-Catalyzed Reduction of Carbon Dioxide to Formate using Formate Dehydrogenase and an Artificial Cofactor, Acc. Chem. Res. 52 (2019) 676–685, https://doi.org/10.1021/acs.accounts.8b00551.

[29] X. Su, H.J. Kulik, T.F. Jamison, T.A. Hatton, Anion-Selective Redox Electrodes: Electrochemically Mediated Separation with Heterogeneous Organometallic Interfaces, Adv. Funct. Mater. 26 (2016) 3394–3404, https://doi.org/10.1002/adfm.201600079.

[30] C. Chen, J.F. Khosrowabadi Kotyk, S.W. Sheehan, Progress toward Commercial Application of Electrochemical Carbon Dioxide Reduction, Chem 4 (2018) 2571–2586, https://doi.org/10.1016/j.chempr.2018.08.019.

[31] J.B. Greenblatt, D.J. Miller, J.W. Ager, F.A. Houle, I.D. Sharp, The Technical and Energetic Challenges of Separating (Photo)Electrochemical Carbon Dioxide Reduction Products, Joule. 2 (2018) 381–420, https://doi.org/10.1016/j.joule.2018.01.014.

[32] M.G. Kibria, J.P. Edwards, C.M. Gabardo, C.T. Dinh, A. Seifitokaldani, D. Sinton, E. H. Sargent, Electrochemical CO2 Reduction into Chemical Feedstocks: From Mechanistic Electrocatalysis Models to System Design, Adv. Mater. 31 (2019) 1–24, https://doi.org/10.1002/adma.201807166.

[33] X. Su, A. Kushima, C. Halliday, J. Zhou, J. Li, T.A. Hatton, Electrochemically-mediated selective capture of heavy metal chromium and arsenic oxyanions from water, Nat. Commun. 9 (2018), https://doi.org/10.1038/s41467-018-07159-0.

[34] A. Dash, R. Chakravarty, Electrochemical separation: Promises, opportunities, and challenges to develop next-generation radionuclide generators to meet clinical demands, Ind. Eng. Chem. Res. 53 (2014) 3766–3777, https://doi.org/10.1021/ie404369y.

[35] X. Su, Electrochemical interfaces for chemical and biomolecular separations, Curr. Opin. Colloid Interface Sci. 46 (2020) 77–93, https://doi.org/10.1016/j.cocis.2020.04.005.

[36] X. Su, T.A. Hatton, Redox-electrodes for selective electrochemical separations, Adv. Colloid Interface Sci. 244 (2017) 6–20, https://doi.org/10.1016/j.cis.2016.09.001.

[37] S. Velmurugan, S. Palanisamy, T.-C.-K. Yang, M. Gochoo, S.W. Chen, Ultrasonic assisted functionalization of MWCNT and synergistic electrocatalytic effect of nano-hydroxyapatite incorporated MWCNT-chitosan scaffolds for sensing of nitrofurantoin, Ultrason. Sonochem. 62 (2020), 104863, https://doi.org/10.1016/j.ultsonch.2019.104863.

[38] B.J. Choudhury, V.S. Moholkar, Ultrasound-assisted facile one-pot synthesis of ternary MWCNT/MnO2/rGO nanocomposite for high performance supercapacitors with commercial-level mass loadings, Ultrason. Sonochem. 82 (2022), 105896, https://doi.org/10.1016/j.ultsonch.2021.105896.

[39] B. Koo, S.P. Jung, Improvement of air cathode performance in microbial fuel cells by using catalysts made by binding metal-organic framework and activated carbon through ultrasonication and solution precipitation, Chem. Eng. J. 424 (2021), 130388, https://doi.org/10.1016/j.cej.2021.130388.

[40] A. Brotchie, D. Borisova, V. Belova, H. Möhwald, D. Shchukin, Ultrasonic modification of aluminum surfaces: Comparison between thermal and ultrasonic effects, J. Phys. Chem. C 116 (2012) 7952–7956, https://doi.org/10.1021/jp3016408.

[41] S. Polat, R. Kortlever, H.B. Eral, Electrochemical cell design and performance evaluation of polyvinyl ferrocene/carbon nanotube electrodes for selective formate separation, Sep. Purif. Technol. 324 (2023), 124554, https://doi.org/10.1016/j.seppur.2023.124554.

[42] S. Polat, R. Kortlever, H.B. Eral, Ultrasound-promoted preparation of polyvinyl ferrocene-based electrodes for selective formate separation: Experimental design and optimization, Ultrason. Sonochem. 89 (2022), 106146, https://doi.org/10.1016/j.ultsonch.2022.106146.

[43] F. He, P.M. Biesheuvel, M.Z. Bazant, T.A. Hatton, Theory of water treatment by capacitive deionization with redox active porous electrodes, Water Res. 132 (2018) 282–291, https://doi.org/10.1016/j.watres.2017.12.073.

[44] F. He, A. Hemmatifar, M.Z. Bazant, T.A. Hatton, Selective adsorption of organic anions in a flow cell with asymmetric redox active electrodes, Water Res. 182 (2020), 115963, https://doi.org/10.1016/j.watres.2020.115963.

[45] M. Gencten, Y. Sahin, A critical review on progress of the electrode materials of vanadium redox flow battery, Int. J. Energy Res. 44 (2020) 7903–7923, https://doi.org/10.1002/er.5487.

[46] R. Zhang, K. Li, S. Ren, J. Chen, X. Feng, Y. Jiang, Z. He, L. Dai, L. Wang, Sb-doped SnO2 nanoparticle-modified carbon paper as a superior electrode for a vanadium redox flow battery, Appl. Surf. Sci. 526 (2020), https://doi.org/10.1016/j.apsusc.2020.146685.

[47] S. Abbas, S. Mehboob, H.J. Shin, O.H. Han, H.Y. Ha, Highly functionalized nanoporous thin carbon paper electrodes for high energy density of zero-gap vanadium redox flow battery, Chem. Eng. J. 378 (2019), 122190, https://doi.org/10.1016/j.cej.2019.122190.